

Effect of Viscous Stress on Cavitation Flow in Nozzles

S. B. Martynov*, D. J. Mason, and M. R. Heikal

Engineering Research Centre, School of Engineering, University of Brighton, BN2
4GJ, Brighton, U.K.

* Corresponding author. Tel.: +44 1273 642331; fax: +44 1273 642301;

e-mail address: S.Martynov@bton.ac.uk

Submitted for publication in the Journal of Fluids Engineering, Trans. ASME, 09 August, 2006

Abstract: A single-fluid approach was applied to study the effect of viscous shear stresses in a cavitating flow. A model of cavitation, based upon the void fraction transport equation was developed and implemented into the PHOENICS computational fluid dynamics code. This model takes into account the variation in the rates of evaporation and condensation with the average viscous shear stresses in fluid. These are calculated using the renormalisation-group (RNG) turbulence model. The cavitation model was adjusted to predict steady flows in models of life-size Diesel injection nozzles. It is concluded that high shear stresses in the liquid delay the collapse of cavitation structures, and have significant effect on the predicted pattern of cavitation flow.

Keywords: *cavitation, modeling, bubbles, scaling, shear stress, tensile strength.*

1. Introduction

1.1. Conventional concept of cavitation

Cavitation is commonly known as the process of formation of voids in a liquid due to a sudden pressure drop, when the local tension $p_v - p$ exceeds the tensile strength of the liquid $p_v - p_{cr}$ [1]. The tensile strength of real liquids, which contain impurities in a form of contaminating particles and small bubbles, is small in comparison to the tensile strength of specially purified liquids. Therefore, in practice, when the cavitation onset is not of a special interest, the cavitation threshold p_{cr} can be associated with the saturation pressure p_v . In flowing liquids, cavitation bubbles formed in a region at low static pressure $p < p_{cr} \approx p_v$ tend to collapse being convected into regions at high pressure $p > p_{cr}$. The process of formation and consequent collapse of bubbles in a liquid is known as the *hydrodynamic cavitation* [2].

1.2. Similarity and scale effects

In experimental practice the hypothesis about hydrodynamic similarity of cavitation flows is applied when attempting to transfer observations from a model to a real-scale flow. This hypothesis becomes useful in design of large ship propellers [2] and miniature Diesel injection nozzles of a sub-millimeter scale [3]. Classical scaling theory [4] states that necessary conditions for the hydrodynamic similarity of two flows are geometrical similarity of the flow domains, equivalence of the dimensionless governing parameters, and initial and boundary conditions for the flow. Experimental studies [5, 6] have confirmed that the Reynolds number Re and

cavitation number CN are the most important criteria, which describe similarity of cavitation flows in nozzles. The present study uses the definition for cavitation number introduced by Bergwerk [5] and applied by Nurick [6] and Soteriou et al. [7]:

$$\text{CN} = \frac{p_1 - p_2}{p_2 - p_v}, \quad (1)$$

where p_1 and p_2 are pressures at the inlet and outlet of nozzle and p_v is the vapor pressure, usually associated with the saturation pressure in the liquid.

Any deviations from the similarity can be interpreted as a result of *scale effects*. Thus, experiments have shown that real flows do not always obey the classical scaling theory due to *scale effects* caused by the liquid quality, bubble dynamics, geometrical differences due to manufacturing and wall roughness, particular flow regime and turbulent motion [3, 5, 6, 8].

The *liquid quality* effects are associated with the presence of dissolved gases in the liquid, small particles and gas-vapor nuclei in the liquid.

The *flow effects* depend on the geometry of the flow domain (*geometry effects*), cavitation number, Reynolds number and parameters of turbulent motion (*viscous effects*). They determine the structure of cavitation-free flow (laminar or turbulent, location of separation point and extent of the recirculation region) and govern the onset and development of cavitation flow.

In practice, to make two cavitation flows similar, the *scale effects* associated with the liquid quality and viscous nature of the flow should be minimized. From the point of view of accurate and reliable prediction of cavitation flows it becomes important to identify and model the scale effects, which determine the particular

regime and properties of cavitation flow. A quantitative description of the flow scale effects requires three-dimensional and transient model of viscous two-phase flow, and a local model of cavitation, which may be incorporated in an appropriate CFD code. In the turn, reliable and similarity consistent model of cavitation would require description of the liquid quality scale effects. Recent progress in understanding of mechanisms of the hydrodynamic cavitation and numerous measurements of cavitation flows published in the literature provide a good basis for development and validation of such model.

In our previous study [9] we have addressed a problem of description of similarity of cavitation flows in liquids with initially present cavitation bubbles. In the present paper we consider the viscous stress scale effect on cavitation flow. This effect arises in high-speed flows, such as flows in Diesel injectors, where shear stresses can contribute to the mechanism of the fracture formation in liquid. Experimental evidences to this phenomenon are rear. In order to clarify the effect of viscous stresses on cavitation flow, we apply measurements of cavitation in liquids of different viscosity. Then we suggest a model for the critical pressure in liquid that takes into account the viscous shear stresses. Preliminary results of this study were submitted to the 13th International Heat Transfer Conference [10].

1.3. Cavitation in a flowing liquid and viscous stress scale effect

The above conventional definition for the cavitation [1] is based upon the observations on liquid rupturing at static or quasi-static conditions, when the hydrostatic pressure in major part of the liquid volume is much higher than the viscous stresses caused by the liquid motion, as, for example, in classical experiment on the tensile strength of liquids [11]. Though this definition is widely used in

predictions of cavitation phenomenon, it does not take into account a mechanism of liquid rupturing by shear stresses.

In incompressible Newtonian liquids, the stress tensor is conventionally written in a form with diagonal elements equal to the hydrostatic pressure defined as mean of the normal stresses $p \equiv -\frac{1}{3} \sum \tau_{ii}$ [4]:

$$\tau_{jk} = -p\delta_{jk} + \underbrace{2\mu \cdot S_{jk}}_{\text{shear stress}},$$

where μ is dynamic coefficient of viscosity, and $S_{jk} = \frac{1}{2} \left(\frac{\partial u_j}{\partial x_k} + \frac{\partial u_k}{\partial x_j} \right)$ is the rate-of-

strain tensor. In a flowing liquid the diagonal components of the stress tensor in principal coordinates are not equal and differ from the hydrostatic part $\sum \tau_{ii} / 3$.

Daniel Joseph has suggested that fracture in liquid can occur when the maximum tension becomes positive [12]:

$$\max(\tau_{ii}) + p_v > 0, \quad (2)$$

where τ_{ii} denotes the principal components of the stress tensor τ_{jk} . Criterion (2) determines the *onset* of cavitation in the flowing liquid.

In two-dimensional shear flow (Fig. 1) the condition (2) can be simplified to [13]:

$$p < \underbrace{p_v + \mu \frac{\partial u}{\partial y}}_{p_{cr}}. \quad (3)$$

Conditions (2) and (3) show that the liquid may start cavitating even when local static pressures are above the saturation pressure $p > p_v$, but viscous stresses are high enough. The criterion (2) generalises the conventional condition $p < p_v$, valid in the limit of “low viscosity” liquid.

Though Daniel Joseph has delivered his hypothesis about the stress-induced cavitation [12] a decade ago, it has not been applied in computational practice. This was caused by the demand in prediction of cavitation flows at relatively low system pressures, when the criterion $p < p_v$ is satisfied. However, description of cavitation in Diesel injectors at “high” system pressures requires revision of the conventional concept $p_{cr} = p_v$.

1.4. Experimental observations

In the limiting case of “low” viscosity liquid condition (2) simplifies to the criterion $p < p_v$. In order to clarify the effect of viscous stresses on the onset of cavitation, it would be helpful to compare the cavitation formation for two flows characterised by the same strain rate, but different viscosity. Analysis of the available experimental data on cavitation flows shows that the data collected by Roosen et al. [14] (as reported by Yaun et al. [15]) on cavitation in water and Winklhofer et al. [16] on cavitation of Diesel fuel, are suitable for this purpose. Here we compare observations of cavitation flows from these publications.

Studies [14] and [16] describe measurements of cavitation flows in nozzles of rectangular shape, formed by steel lamellas placed in between the two pieces of glass. Though the nozzle manifolds had different shapes (Fig. 2), and nozzle widths W were

slightly different (0.2 mm in [14], and 0.3 mm in [16]), the nozzle heights H were very similar (0.28 mm in [14], and 0.299 mm in [16]), and the nozzle lengths L were exactly the same (1 mm). Also, the roundness of the nozzle entry r_{in} , which results from the imperfections in the manufacturing of the nozzles, was estimated in both cases to be of the same order of magnitude ($30 \mu\text{m}$ in [14], and $20 \mu\text{m}$ in [16]).

Consideration of the images of cavitation flows reported by Roosen et al. [14] and Winklhofer et al. [16] (Table 1) reveals very similar cavitation vapor structures. Thus, under pressure difference around 5.8 MPa both authors have observed a vapor pocket at the nozzle entry (inlet cavitation). For the pressure drop about 6.9 MPa, Roosen et al. [14] have observed super-cavitation flow, and Winklhofer et al. [16] have reported critical cavitation with the transition to super-cavitation flow at 6.6 MPa. Remarkably, the system pressures (downstream of the nozzle exit) were completely different in these studies (1.1 and 2.1 MPa in [14], and 3.4 and 4.3 MPa as reported in [16]).

Comparison of the flow patterns in Table 1 shows that cavitation structures effectively depend upon the pressure difference $p_1 - p_2$, that means that the cavitation number CN is not a sufficient criterion to describe the development of cavitation. Assuming the liquid quality and the pressure and velocity fields are similar for both flows (Reynolds numbers Re_H in Table 1 indicate that the flows are highly-turbulent in all the cases), the difference in pressure levels required to produce similar cavitation structures can be attributed to the viscous effects. While the density of Diesel fuel $\rho_l = 840 \text{ kg/m}^3$ is of the same order of magnitude of the density of water $\rho_l = 1000 \text{ kg/m}^3$, the dynamic viscosity of Diesel fuel $\mu_l \approx 0.003 \text{ Pa} \cdot \text{s}$ is nearly three times bigger than the viscosity of water $\mu_l \approx 0.001 \text{ Pa} \cdot \text{s}$. This may cause shear

stresses that are three times higher in the flow of Diesel fuel compared to water flow at the same strain rates. According to hypothesis (2), the viscous stress can influence the critical pressure threshold for the cavitation onset. This hypothesis can explain why the cavitation starts at lower system pressures in the flow of Diesel fuel, than in the water flow case.

1.5. Objectives of the study

In order to predict the steady-state patterns of cavitation flows experimentally established in [14] and [16], we perform numerical simulations using CFD method. Many observations have proved that the *hydrodynamic cavitation* occurs in the *bulk* liquid [1], where the vapor-gas bubbles provide the main contribution to the nucleation process. Therefore we decided to use a model of cavitation flow based on the bubble-dynamics theory. Applying a conventional concept $p_{cr} \approx p_v$ to the relatively low-pressure cavitation flow of water [14] and relatively high-pressure flow of Diesel fuel [16], we identify the problem of describing cavitation flows at high system pressures, when cavitation can be affected by viscous stress. To resolve this problem, a cavitation model, which accounts for the viscous-stress scale effect, is suggested and applied to describe the measurements. It is worth noting that the literature survey has not revealed any models of cavitation which account for the shear stress mechanism of cavitation.

2. Model of Cavitation Flow

2.1. Model for liquid-vapor flow

In our study it has been assumed that the liquid-vapor mixture can be described in terms of two inter-penetrating continua. Thus, the flow may be simulated as either a “multi-phase” (separate velocity vectors for the liquid and vapor), or a “single phase” (one velocity vector) flow. The following simplifying assumptions have been made, there is no slip between the continua, and the continua are in thermal equilibrium. Thus the mixture can be considered as a “single phase” with its physical properties varying according to the local concentration of liquid and vapor. The set of governing equations, which describes steady-state flow of the mixture in Cartesian coordinates is as follows:

$$\frac{\partial \rho u_j}{\partial x_j} = 0, \quad (4)$$

$$\frac{\partial \rho u_i u_j}{\partial x_j} = -\frac{\partial p}{\partial x_i} + \frac{\partial \tau_{ij}}{\partial x_j}, \quad (5)$$

where $\tau_{ij} = (\mu + \mu_t) \cdot \left(\frac{\partial u_i}{\partial x_j} + \frac{\partial u_j}{\partial x_i} - \frac{2}{3} \delta_{ij} \frac{\partial u_k}{\partial x_k} \right)$.

The flow is considered to be incompressible, with the properties of the liquid and vapor being constant. The mixture properties are taken to be [15]:

$$\rho = \alpha \rho_v + (1 - \alpha) \rho_l, \quad (6)$$

$$\mu = \alpha \mu_v + (1 - \alpha) \mu_l. \quad (7)$$

where α is the volume fraction of the vapor.

Equations (4) and (5) should be completed by the initial and boundary conditions, and equations for calculation of the turbulent viscosity μ_t of the mixture and the void fraction α . The model for calculation of the void fraction in cavitation flow is described in the following section.

For accurate prediction of turbulent flow in nozzles with flow separation, the RNG $k - \varepsilon$ model by Yakhot and Orzag [17] was applied in our study.

2.2. Model for cavitation

The present study is based on a single-fluid cavitation model [15], which has been developed under several assumptions about the nature of the cavitation phenomenon. First, the flow is described assuming a local homogeneous mixture of the vapor and liquid phases. This concept neglects the actual shape of the cavitation pockets and uses the void fraction to quantify the local content of vapor in the flow. Second, to calculate the void fraction, a transport equation is introduced [15]. In this equation the rates of evaporation and condensation are derived using an analogy with the growth and decay of spherical bubbles in liquid. To make the homogeneous concept valid, these bubbles should be small, so that their motion relative to the liquid can be neglected.

2.2.1. Void fraction

The current approach assumes that cavitation can be described locally for bubbles of one sort, characterized by size and number density per volume of liquid. The volume fraction of the vapor can then be computed from the number density and radius of these virtual bubbles:

$$\alpha = \frac{n \frac{4}{3} \pi R^3}{1 + n \frac{4}{3} \pi R^3}. \quad (8)$$

2.2.2. Bubble radius

To estimate the rates of growth and collapse of bubbles, the linear model by Rayleigh [8], is applied:

$$\frac{dR}{dt} = \sqrt{\frac{2}{3} \frac{|p_v - p_l|}{\rho_l}} \cdot \text{sign}(p_v - p_l), \quad (9)$$

where p_v – is vapor pressure, associated with the pressure inside the bubble, and p_l is pressure in the surrounding liquid, approximately equal to pressure in the mixture $p_l \approx p$. This model can be considered as a limiting case of the Rayleigh-Plesset equation, when the effects of surface tension, liquid viscosity and inertia of the bubble are neglected.

To initiate cavitation, bubble nuclei of radius R_o are assumed to be present in the liquid.

2.2.3. Transport equation for the void fraction

Following [15], the transport equation for the void fraction α is derived from Eq. (8) under the assumptions of constant densities of the vapor and the liquid and fixed number density of cavitation bubbles in the flow domain:

$$\frac{\partial \alpha}{\partial t} + \frac{\partial u_j \alpha}{\partial x_j} = S_\alpha, \quad (10)$$

where the source term is given by the equation:

$$S_\alpha = \frac{(1-\alpha)\rho_l}{\rho} \cdot \frac{n}{1+n \cdot \frac{4}{3}\pi R^3} \cdot \frac{d}{dt} \left(\frac{4}{3}\pi R^3 \right). \quad (11)$$

2.2.4. Parameters of the model

A common strategy in computation of cavitation flows is to tune parameters of a model using some reference measurements of cavitation, and then apply these set of constants for a range of the flow conditions. Thus, the model of Yaun et al. [15] contains two adjustable parameters R_o and n , which describe the *liquid quality* effects on a cavitation flow. The number density n plays a role of tunable parameter for matching reference measurements, while the initial bubble radius is aimed to activate the source term in Eq. (10).

A weakness of this approach is that the number density is not a function of the liquid quality only, but depends also on the hydrodynamics of the flow [9]. In order to decouple these two effects a model for the concentration of cavitation nuclei has been developed [9]. This model was aimed to predict cavitation flows of a given liquid for arbitrary flow configuration. In the current study we apply the original model by Yuan et al. [15] to study cavitation of different liquids in similar flow conditions.

In our study the number density parameter n and the vapor pressure p_v in the source term (11) are considered as fixed parameters, which depend on the liquid quality and can not be affected by the cavitation number. The vapor pressure p_v is set

to 2340 Pa for water and 300 Pa for Diesel fuel. The initial radius of cavitation bubbles is specified through the number density n and initial volume fraction of the vapor phase, which is setup to a small number $\alpha_o = 10^{-8}$. This value was found to have no effect on the resultant flow field, but is needed to activate the source term Eq. (11).

2.3. Numerical method

In this study the PHOENICS CFD code [19] is employed as an instrument to solve the set of governing Eqs. (4 – 10) completed by boundary flow conditions and equations of a turbulent model, using the finite-volume method [20]. The model of cavitation described in the previous section was incorporated into the package.

In order to improve the accuracy of computations on coarse meshes, high-order convection discretization schemes were applied when solving the mass fraction equation (super-bee scheme) and the momentum equation (SMART scheme) [21]. To promote convergence of pressure-solution algorithm for computation of flows with large density gradients, an artificial compressibility factor was introduced in the calculations.

2.4. Mesh and boundary conditions

Discretization of the differential equations is performed on a body-fitted grid built for one quarter of the nozzle in between the symmetry planes, back plane wall and curvilinear nozzle side wall (Fig. 3). For the straight part of the nozzle, starting from its inlet corners, a Cartesian grid was used. In the calculations meshes with about 2500 cells in computational domain were applied.

The velocity of the flow is specified and the turbulent intensity is set to zero at the inlet of the domain (Fig. 2). At the outlet of the nozzle, a constant pressure boundary condition is applied. At the nozzle walls the no slip boundary condition was applied for the velocity components. The boundary conditions for the momentum equation were formulated using the standard equilibrium wall functions.

2.5. Convergence of iterations

Numerical tests revealed that in order to minimize the residuals and achieve the flow fields, which have virtually stopped varying with the iterations, 10^4 global iterations of solution algorithm were sufficient for computations on a coarse mesh (Fig. 3). Calculations for one flow regime on a personal computer with Pentium 4 processor with operating frequency 2.66 GHz took approximately one hour. Most simulations were started with initial flow fields based upon the converged solution when cavitation is neglected. Variation of the initial flow fields was found to have no effect on the final flow field (as would be expected for a steady state flow), but did significantly reduce computation time. The results of a mesh dependence study showed that the use of high-order spatial discretization schemes applied for approximation of advection terms in the mass fraction and momentum equations, allowed accurate results to be obtained using coarse meshes (Fig. 3).

3. Results

In order to clarify the nature of the shear-stress-assisted cavitation, the measurements by Roosen et al. [14] and Winklhofer et al. [16] were considered. In this part, by comparison of the numerical results with the measurements, the problem in application of the conventional model of cavitation is identified. Then, the method

to account for the effect of viscous shear stresses on cavitation flow is introduced and applied to describe the experimental data.

3.1. Conventional concept

3.1.1. Cavitation of tap water in Roosen's nozzle

In order to describe cavitation flows of tap water [14], the parameter n was tuned for the reference regimes from Table 1. This was done following the procedure described by Yaun et al. [15], using the conventional definition for the cavitation pressure threshold ($p_{cr} = p_v$).

Inlet cavitation. First, adjustment of n was performed for the inlet cavitation flow. After a number of trials, it was found that number densities from $n = 1.6 \cdot 10^{13} (\text{m}^{-3})$ to $n = 2 \cdot 10^{15} (\text{m}^{-3})$ produce vapor pockets at the nozzle entrance, which can be associated with the cavitation bubble photographed by Roosen et al. [14]. The following results are discussed for the value $n = 4.4 \cdot 10^{14} (\text{m}^{-3})$, which was chosen as a result of the model adjustments to achieve best agreement with the measurements for both the inlet and super-cavitation flows.

Fig. 4 shows the distribution of the volume fraction of vapor, predicted using $n = 4.4 \cdot 10^{14} (\text{m}^{-3})$, in comparison with the image of the flow from the report by Roosen et al. [14]. The void fraction field shows high concentrations of vapor (more than 50%) in the cavitation region and steep gradients of concentration, which indicates a small numerical diffusion effect.

Fig. 5 shows results of the calculation of the velocity field in the middle X-plane of the nozzle in comparison with the velocity measurements performed by Roosen et al. [14]. The shape of the vapor pockets predicted by the model are indicated in this

figure by iso-surfaces of the void fraction $\alpha = 20\%$. Though the shape of the vapor pocket predicted numerically does not match precisely the measurements, it captures the phenomena of inlet cavitation. The numerical study have revealed that to describe correctly the regime of inlet cavitation, concentration of cavitation bubbles n must not exceed $4.4 \cdot 10^{14} (\text{m}^{-3})$. Further increase in n resulted in a shift of the reattachment point downstream the flow, which is typical for *transitional* cavitation and does not correspond to the *sub-cavitation* regime [22] with steady-state inlet vapor pocket reported by Roosen et al. [14].

Supercavitation. As already mentioned, the number density parameter n was adjusted with the help of the measurements of supercavitation flow (CN = 6.27, Table 1). This was done to identify the value of n more precisely. When applying the measurements of the super-cavitation flow regime, we assumed that it can be associated with “critical” cavitation, when the length of the vapor pocket just reaches the nozzle outlet.

The results of calculations of the void fraction are shown in Fig. 6 for the number density $n = 4.4 \cdot 10^{14} (\text{m}^{-3})$, which was found to be the minimal value that can predict the super-cavitation shape of the vapor pocket.

3.1.2. Cavitation of Diesel fuel in Winklhofer’s nozzle

The model of cavitation developed by Yaun et al. [15] was able to predict both the inlet and developed (super-cavitation) flows, such as those experimentally observed by Roosen et al. [14], using one value for the number density of cavitation bubbles n . In order to describe the regimes of cavitation of Diesel fuel in Winklhofer’s nozzle (Table 1), the parameter n has been adjusted once again.

However, first attempts to find an appropriate value of n showed that for both of the regimes (inlet cavitation and super-cavitation), the model predicted very tiny cavitation areas located at the nozzle inlet corner, even when very high concentrations of nuclei $n \sim 10^{20} (\text{m}^{-3})$ were specified. Thus, for the super-cavitation flow, the length of the vapor pocket does not exceed a length of a nozzle height, irrespective of the number density n (Fig. 7). Calculations using finer mesh did not change the results. The reason for such discrepancy between the numerical predictions and the measurements could be the shear stress mechanism of cavitation, which was not considered in the conventional concept $p_{cr} = p_v$, adopted in the model of cavitation. The following analysis is aimed to clarify this issue.

3.2. Pattern of cavitation-free flow

In order to reveal the differences in flows of tap water in Roosen's nozzle and Diesel fuel in Winklhofer's nozzle, the calculations were performed neglecting the cavitation process for the pressure drops across the nozzle around 5.8 MPa (inlet cavitation, Table 1). Analysis of the liquid flow fields results with a model for the critical pressure influenced by the viscous shear stress.

Fig. 8 shows the pressure distributions along the nozzles. Though the shapes of the pressure curves are different, the overall pressure drop $p_1 - p_2$ and maximum pressure reduction at the nozzle entry $p_2 - p_{\min}$ are similar for the two nozzles. This can be explained by the similar geometry scales and negligible viscous losses under the turbulent flow conditions (Table 1).

Figs. 9 – 13 and 15 show spatial distributions for the flow variables under cavitation-free flows, for the middle cross-sections ($X = 0$) of the nozzles.

Fig. 9 shows that the mean flow velocity scales were similar in both nozzles, as they were determined by the pressure drop, although the flow fields were different in detail.

The blank spots at the nozzle inlet corners in Fig. 10 show the area of the flow where pressure becomes negative (the relative pressure $p - p_2$ drops below the level $-p_2$), see also Fig. 8). These regions indicate the volume of liquid subjected under tension $p_v - p > 0$. Comparison of Fig. 10 (a) and (b) reveals a larger volume of liquid under tension for the Roosen's nozzle, where the flow is characterized by a lower exit pressure p_2 .

Comparison of Figs. 11 (a) and (b) shows similar distributions for the rates of strain

$$S_{yz} = \frac{1}{2} \left(\frac{\partial u_z}{\partial y} + \frac{\partial u_y}{\partial z} \right). \quad (12)$$

and approximately the same maximum level of strains achieved for both nozzles. At the same time, the higher viscosity of the Diesel fuel results in higher shear stresses (Fig. 12, b). In the turn, according to the hypothesis (2), higher stresses can result in lower critical pressures for the onset of cavitation.

Fields of the turbulent viscosity (Fig. 13) show that the average turbulent stresses prevail over the laminar stresses near the wall downstream the nozzle entrance, i.e. in those regions of the flow where the cavitation is expected to happen. In order to apply criterion (2) in the framework of the Reynolds-averaged Navier-Stokes equations, the contribution from the averaged turbulent stresses have to be appreciated in (2). Taking into account that flows in the nozzles are effectively two-

dimensional, the cavitation criterion can be formulated in a form (3), with the critical pressure defined as:

$$p_{cr} = p_v + 2 \cdot (\mu + \mu_t) \cdot S_{ij}^{\max}, \quad (13)$$

where S_{ij}^{\max} is the maximum component of the strain-rate tensor.

Fig. 12 (b) indicates that the local maximum in shear stress takes place at about one half of the nozzle height downstream the nozzle inlet where the pressure already recovers to positive values ($p - p_2 > -p_2$, Fig. 10, b). However, the level of the shear stresses in the flow is not sufficient to overcome the hydrostatic pressure p and thus initiate the cavitation. This is schematically shown in Fig. 14.

To complete the analysis, it is interesting to compare the current method of definition of the critical pressure (13) to the model developed by Singhal et al. [23] that accounts for the effect of the turbulent pressure fluctuations in the following way:

$$p_{cr} = p_v + 0.39 \frac{1}{2} \rho k. \quad (14)$$

Equation (14) has an empirical nature and contains tunable constant 0.39. Inspection of the turbulence kinetic energy k fields in cavitation-free flows in the nozzles (Fig. 15) reveals higher level of k reached in the flow separation region in the Winklhofer's nozzle (Fig. 15, b). The kinetic energy of turbulence k is formed under the effect of stresses in liquid, and therefore correlation (14) can be explained on the basis of the model (13).

3.3. Model for the critical vapor pressure

In order to activate the shear-stress mechanism of cavitation described in Eq. (13), the shear stress term in this equation can be magnified by an empirical constant $C_t > 1$:

$$p_{cr} = p_v + 2\mu \cdot \left(1 + C_t \frac{\mu_t}{\mu} \right) \cdot S . \quad (15)$$

Analysis of the liquid flow patterns in Roosen's and Winklhofer's nozzles have revealed that the hypothesis expressed in Eq. (13) can be applied to explain the effect of the viscous shear stress on the cavitation onset. In the present study this idea, in a form of Eq. (15), is used to define the critical pressure threshold for both the evaporation and condensation stages of cavitation.

In the following sections the coefficient C_t is adjusted using the measurements of cavitation flows from Table 1. The study is completed by an analysis of the sensitivity of the results of calculation of cavitation flows to variations in C_t .

3.3.1. Cavitation of water flow in Roosen's nozzle

First, the model for the critical pressure (15) was applied to describe cavitation of tap water (Table 1). The purpose of this step was to determine the maximum value of C_t , which would not affect the cavitation structures predicted assuming $p_{cr} = p_v$. As a result of several computational trials, it was found that application of Eq. (15) with a constant $C_t \leq 10$, does not change the solutions for the inlet and developed cavitation in the Roosen's nozzle (Table 1). This is shown in Fig. 16, which gives the

void fraction fields predicted for the inlet and super-cavitation flows in Roosen's nozzle. Then, $C_t=10$ was applied to predict the flow regimes in Winklhofer's nozzle (Table 1).

3.3.2. Cavitation of Diesel fuel in Winklhofer's nozzle

The results of adjustments of the number density n for inlet and critical cavitations in Winklhofer's nozzle (Table 1) using $C_t=10$, are shown in Fig. 17. For the inlet cavitation calculations have revealed that $C_t=10$ does not have a noticeable effect on the dimensions of the vapor region, so that the vapor region (Fig. 17, *a*) kept the same as it was predicted by assuming $p_{cr} = p_v$. Under super-cavitation flow conditions the effect of the number density of cavitation bubbles became more obvious (Fig. 17, *b – d*). An increase in the number density of cavitation bubbles resulted in an elongation of the vapor region and higher concentrations of the vapor phase. Using $n = 2 \cdot 10^{18} \text{ (m}^{-3}\text{)}$ and $n = 1.6 \cdot 10^{19} \text{ (m}^{-3}\text{)}$ the model predicted the cavitation pocket, which occupied about one half of the nozzle length (Fig. 17, *c* and *d*). This shape is in good agreement with experimental observations for the critical cavitation (Table 1). An increase in C_t resulted in a greater amount of vapor being produced in the nozzle. Thus, when using $C_t = 20$, the model predicted the super-cavitation flow pattern, similar to the one reported by Winklhofer et al. [16] (Table 1). At the same time, unique number $C_t = 10$ allowed to describe both the incipient and critical cavitation flows from experiments [14] and [16]. The difference in values of parameter n used to predict cavitation in Roosen's and Winklhofer's nozzles can be explained by dependence of n on the liquid tension $p_{cr} - p$ [9], which according to

concept (3) can be much affected by viscous shear stresses. This issue is above the scope of the present study and requires further investigations.

3.3.3. Analysis of tensions in the liquid

In order to identify the area of cavitation flow influenced by the shear stresses, the spatial distributions of the second term of Eq. (15) $2\mu \cdot \left(1 + C_t \frac{\mu_t}{\mu}\right) \cdot S$ and the local pressure p are compared in Fig. 18. Analysis of the pressure field shows that positive tensions $p_v - p > 0$ and $p_{cr} - p > 0$ appear at the nozzle wall downstream the inlet corner (Fig. 18, *a, b*). However, application of the criterion (15), results in larger volume of liquid where the pressure is reduced below the critical level $p < p_{cr}$ (Fig. 18, *b*). Also, comparison of the distributions of $p - p_v$ and $p - p_{cr}$, shows that the local pressure recovers much faster than the variable $p - 2\mu \cdot \left(1 + C_t \frac{\mu_t}{\mu}\right) \cdot S$ in the mean flow direction (Fig. 18, *c, d*). This leads to the lower rates of condensation and the longer vapor pockets predicted by the model (15) (Fig. 17, *c, d*) compared to the predictions of the conventional concept $p_{cr} = p_v$ (Fig. 7, *b, c*).

4. Conclusions

The effect of the shear-stress mechanism of cavitation was clarified from analysis of the patterns of cavitation flows of tap water [14] and Diesel fuel [16] in planar nozzles.

The results of calculations showed that the conventional concept $p_{cr} = p_v$ fails to predict regimes of cavitation of Diesel fuel, experimentally observed in [16].

In order to account for the effect of shear stresses on cavitation flow, the modeling equation (15) for the critical pressure was introduced. This critical pressure was used to calculate the rates of evaporation and condensation in the flow. An empirical constant C_t in the correlation (15) was adjusted to describe the inlet and critical cavitation flows observed in the experiments [14] and [16].

Analysis of distributions of the flow variables showed that regions where the static pressure reaches its minimum and where the shear stress achieves its maximum are located in different parts of the flow. The calculations showed that larger amount of vapor predicted using Eq. (15), comparing to the conventional model $p_{cr} = p_v$, is a result of two effects: 1) an increase in the rate of evaporation at the nozzle inlet, and 2) a decrease in the rate of condensation downstream the inlet.

5. Acknowledgements

The authors are grateful to the European Regional Development Fund Franco-British INTERREG IIIa (Project Ref. 162/025/247) for partial financial support of the project, and Dr. Tao Bo from Ricardo UK for the initiation of this study.

Figure captions

Fig. 1. Couette flow between two flat plates.

Fig. 2. Planar nozzles used in studies of cavitation flows by Roosen et al. [14], (a), and Winklhofer et al. [16], (b).

Fig. 3. The structure of body-fitted meshes in the Y - Z plane of the computational domain for Roosen's (a) and Winklhofer's (b) nozzles (Fig. 2).

Fig. 4. Pattern of cavitating flow in Roosen's nozzle at $CN = 2.81$ (Table 1) (a) in comparison with the results of numerical predictions of the vapor field using $n = 4.4 \cdot 10^{14} (\text{m}^{-3})$ (b).

Fig. 5. Measured velocity field and shape of the vapor pocket in cavitating nozzle [14] at $CN = 2.81$ (a) in comparison with the results of numerical calculations using $n = 4.4 \cdot 10^{14} (\text{m}^{-3})$ (b). The volume of calculated cavitation region is indicated by iso-surface where the void fraction is $\alpha = 20\%$.

Fig. 6. Pattern of cavitation flow in Roosen's nozzle at $CN=6.27$ (Table 1) in comparison with the results of numerical predictions of the vapor volume fraction field using $n = 4.4 \cdot 10^{14} (\text{m}^{-3})$ (b).

Fig. 7. The void fraction distributions predicted for the supercavitation flow in Winklhofer's nozzle (Table 1) using the model of cavitation by Yuan et al. [15]. (a) $n = 1.6 \cdot 10^{16} (\text{m}^{-3})$, (b) $n = 2 \cdot 10^{18} (\text{m}^{-3})$, (c) $n = 1.6 \cdot 10^{19} (\text{m}^{-3})$, (d) $n = 1.6 \cdot 10^{22} (\text{m}^{-3})$. (Figures show only the right half of the nozzle).

Fig. 8. Pressure distributions in liquid estimated neglecting cavitation for the inlet cavitation regimes in Roosen's and Winklhofer's nozzles (Table 1). Continuous and stroke lines show pressure distribution along near the wall and along the center-line of nozzles, respectively.

Fig. 9. Velocity fields in Roosen's (a) and Winklhofer's (b) nozzles predicted neglecting the cavitation process. (Figures show only the right half of the nozzles).

Fig. 10. Fields of relative pressure $p - p_2$ predicted for Roosen's (a) and Winklhofer's (b) nozzles neglecting the cavitation process.

Fig. 11. Distributions of the component of the rate of strain S_{yz} in Roosen's (a) and Winklhofer's (b) nozzles predicted neglecting the cavitation process.

Fig. 12. Distributions of the shear stresses $\tau_{yz} = 2(\mu + \mu_t)S_{yz}$ in Roosen's (a) and Winklhofer's (b) nozzles predicted neglecting the cavitation process.

Fig. 13. Distributions of coefficient of the turbulent viscosity in Roosen's (a) and Winklhofer's (b) nozzles predicted neglecting the cavitation process.

Fig. 14. Variations in absolute pressure and the turbulent component of shear stresses along the nozzle (schematically).

Fig. 15. Distributions of the kinetic energy of turbulence in Roosen's (a) and Winklhofer's (b) nozzles predicted neglecting the cavitation process.

Fig. 16. Distributions of the void fraction in the Roosen's nozzle under inlet (a, b) and super-cavitation (c, d) flow regimes (Table 1), predicted using $n = 4.4 \cdot 10^{14} \text{ (m}^{-3}\text{)}$. (a, c) – $p_{cr} = p_v$; (b, d) – equation (15) with $C_t = 10$.

Fig. 17. Distributions of the void fraction at the nozzle throat for the inlet cavitation (a) and supercavitation flows (b - d) in Winklhofer's nozzle (Table 1), predicted using equation (15) with a constant $C_t = 10$ and various number densities of cavitation bubbles $n \text{ (m}^{-3}\text{)}$: (a), (c) – $2 \cdot 10^{18}$, (b) – $1.6 \cdot 10^{13}$, (d) – $1.6 \cdot 10^{19}$.

Fig. 18. Iso-surfaces for the tension $p - p_v$ (a, c) and local variable $p - p_{cr}$ (b, d), predicted using equation (15) with $C_t = 10$ and $n = 2 \cdot 10^{18} \text{ (m}^{-3}\text{)}$. (a) $p - p_v < 0$; (b) $p - p_{cr} < 0$; (c) $p - p_v < 4 \cdot 10^5 \text{ (Pa)}$; (d) $p - p_{cr} < 4 \cdot 10^5 \text{ (Pa)}$. (Flow from right to left around the nozzle inlet corner).

Figures

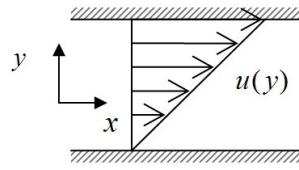
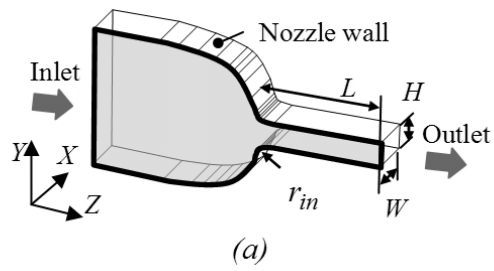
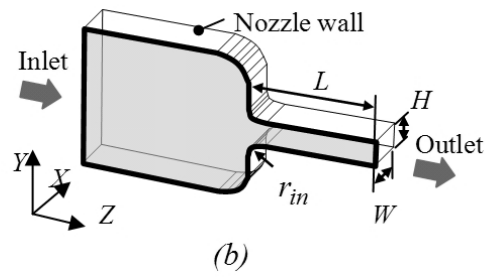


Fig. 1

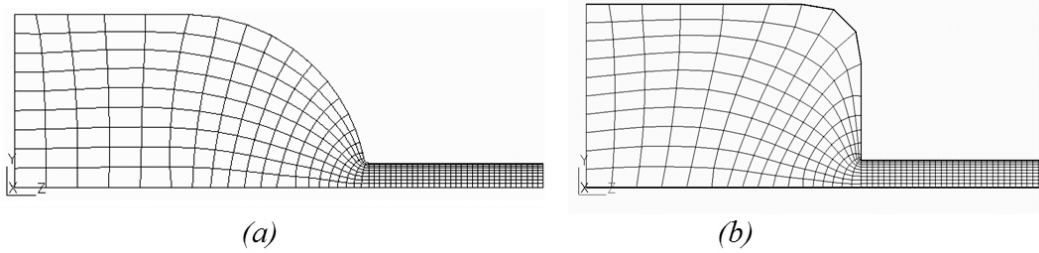


(a)



(b)

Fig. 2



(a)

(b)

Fig. 3

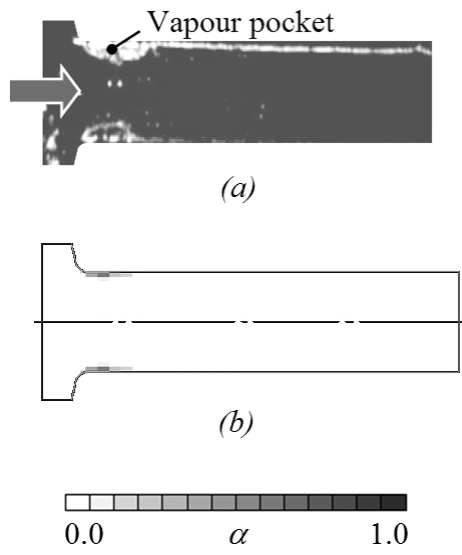


Fig. 4

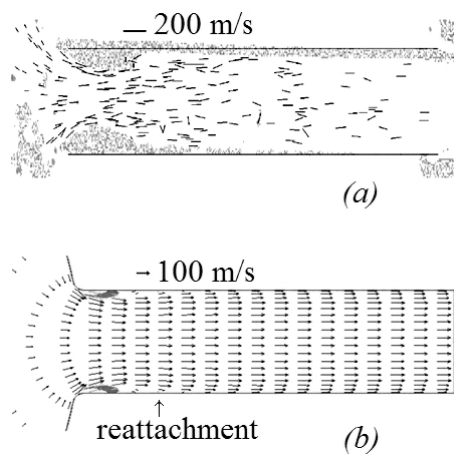


Fig. 5

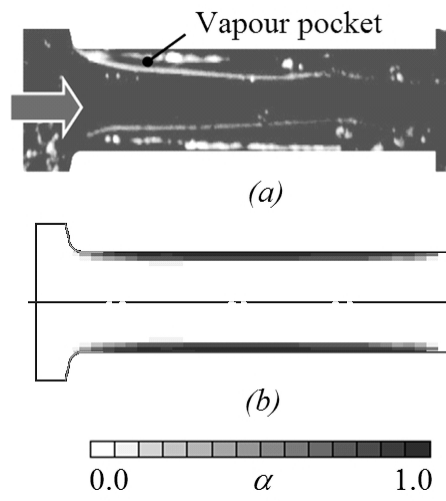


Fig. 6

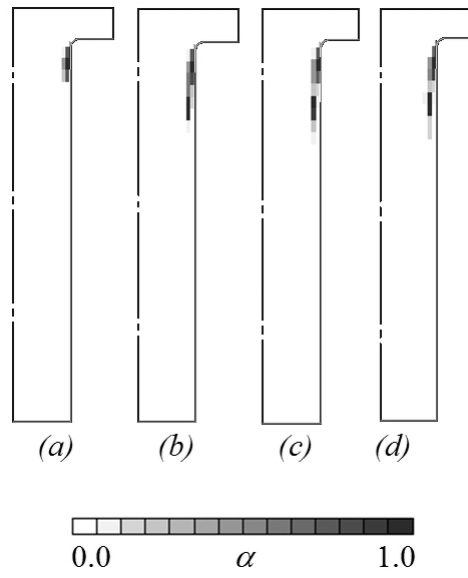


Fig. 7

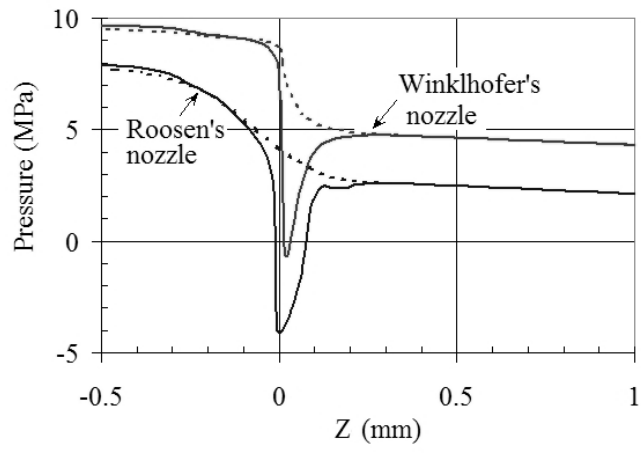


Fig. 8

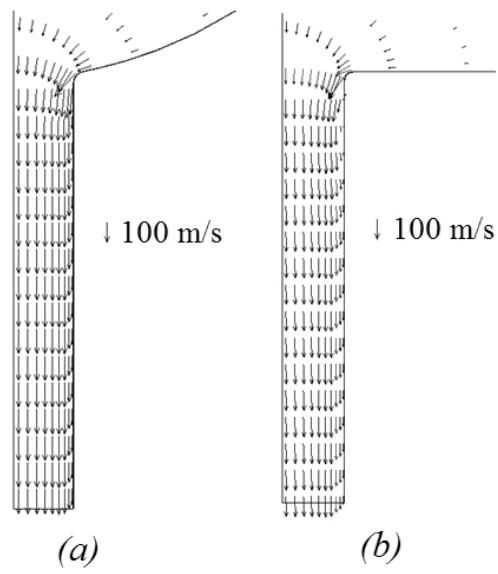


Fig. 9

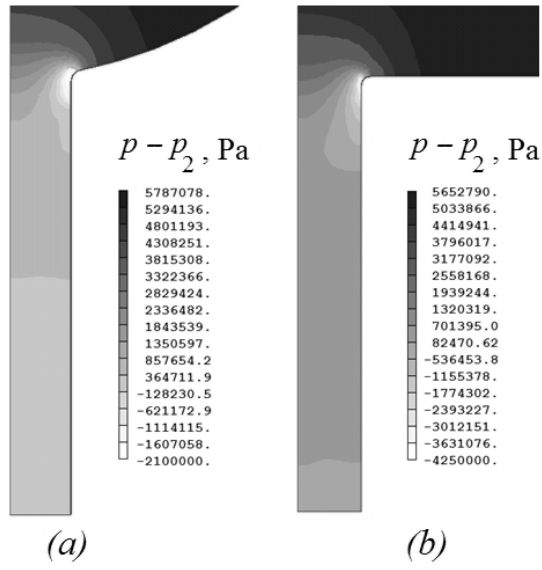


Fig. 10

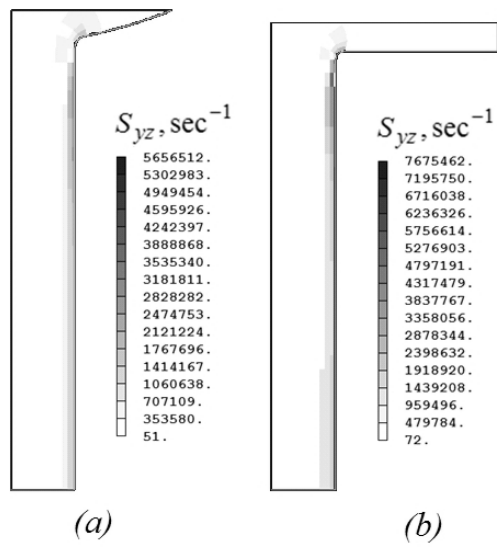


Fig. 11

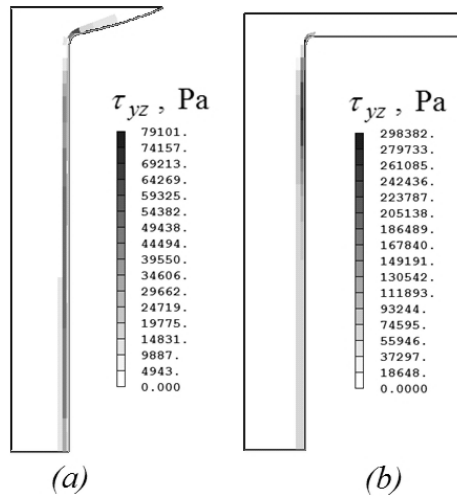


Fig. 12

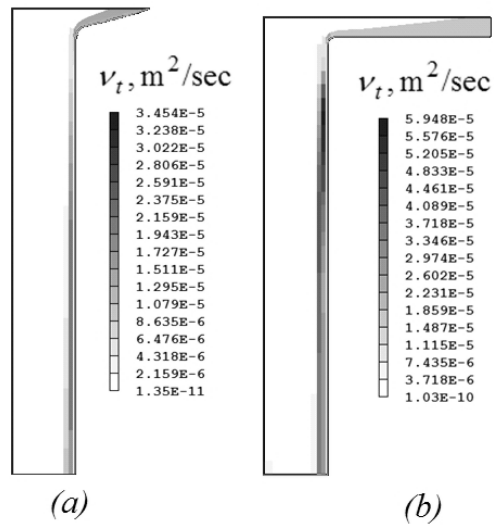


Fig. 13

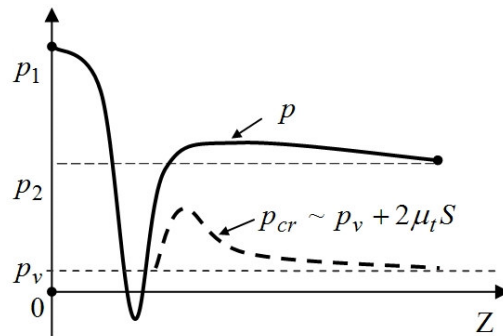


Fig. 14

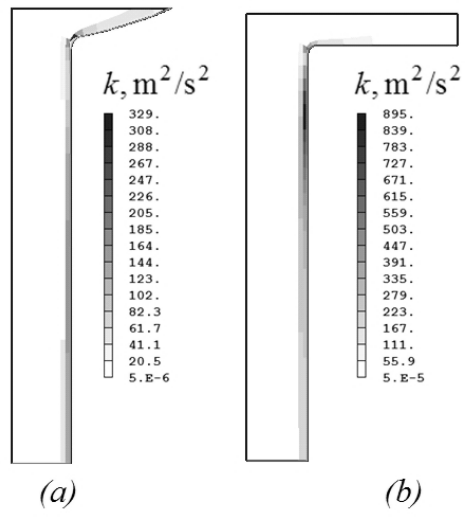


Fig. 15

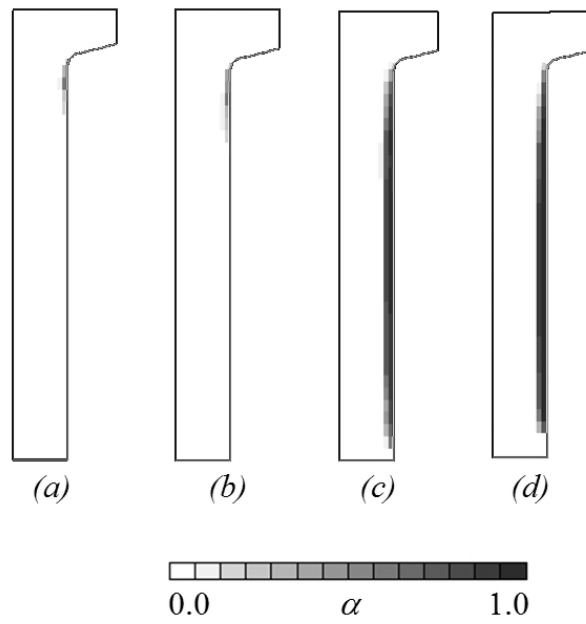


Fig. 16

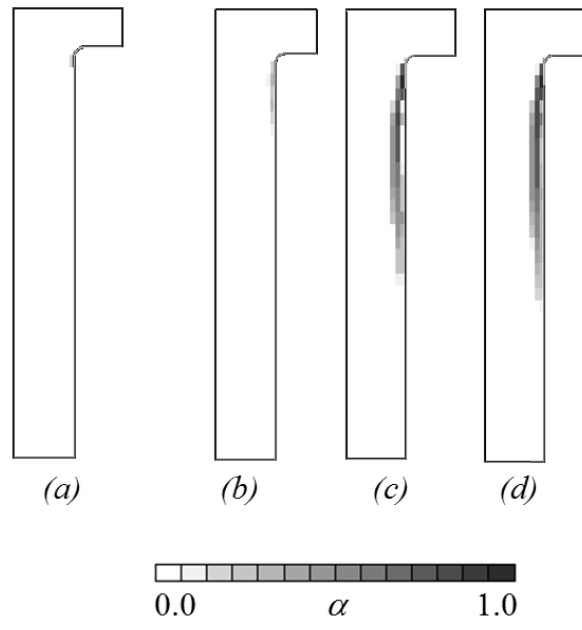


Fig. 17

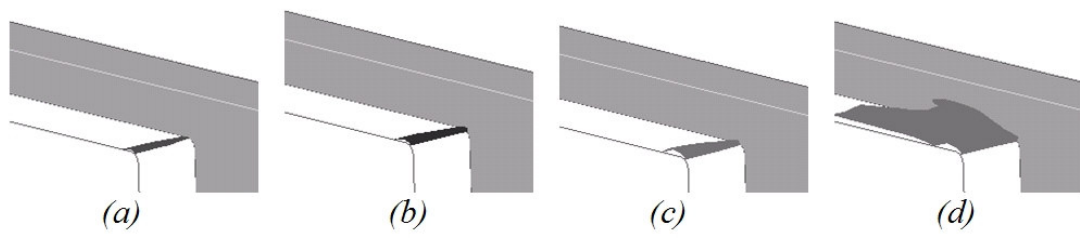


Fig. 18


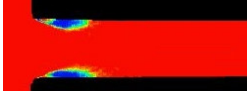

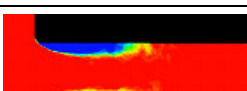
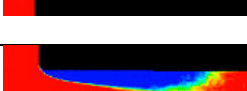
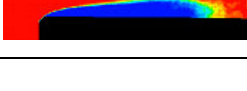
Flow	Authors	Liquid	Images of the flow	p_1 , MPa	p_2 , MPa	$p_1 - p_2$, MPa	CN	Re_H
Inlet cavitation	Roosen et al, (1996)	Water		8	2.1	5.9	2.81	30 400
	Winklhofer, et al. (2001)	Diesel fuel		10	4.3	5.7	1.33	9 800
Super-cavitation	Roosen et al, (1996)	Water		8	1.1	6.9	6.27	32 820
	Winklhofer, et al. (2001)	Diesel fuel		<i>Critical cavitation</i>				
				10	3.5	6.5	1.86	10 450
				10	3.4	6.6	1.95	10 540

Table 1. Developing and super-cavitation flows in rectangular models of Diesel injectors. Comparison of the measurements by Roosen et al. [14] and Winklhofer et al. [16]. Reynolds number $Re_H = \frac{\rho U H}{\mu}$ is defined using the Bernoulli velocity scale $U = \sqrt{2(p_1 - p_2) / \rho_1}$.

Nomenclature

C_t – empirical constant in Eq. (15);

CN – cavitation number defined in Eq. (1);

H – nozzle height, m;

k – kinetic energy of turbulence, m^2/s^2 ;

L – nozzle lengths, m;

n – number density of bubbles in liquid, m^{-3} ;

p – hydrostatic pressure, Pa;

p_{cr} – cavitation pressure threshold, Pa;

p_v – saturation pressure in liquid, Pa;

R – bubble radius, m;

r_{in} – roundness of the nozzle entry, m;

Re – Reynolds number;

S_{jk} – the rate-of-strain tensor, s^{-1} ;

S_α – the source term in Eq. (10), s^{-1} ;

t – time, s;

u_i – velocity components, m/s;

W – nozzle width, m;

X, Y, Z – coordinates, m;

Greek letters

α – volume fraction of the vapor;

δ_{ij} – Kroneker delta tensor;

ε – rate of dissipation of the kinetic energy of turbulence, m^2/s^3 ;

μ – dynamic coefficient of viscosity, Pa s;

ρ – density, kg/m^3 ;

τ_{jk} – stress tensor, Pa;

Subscripts

i, j, k – indexes of coordinates (1,2,3);

cr – cavitation threshold;

l – liquid phase;

o – bubble nuclei;

t – turbulent;

v – vapor phase;

1 – nozzle inlet;

2 – nozzle outlet.

References

- [1] Brennen, C.E., 1995. *Cavitation and Bubble Dynamics*. Oxford University Press, Oxford.
- [2] Knapp, R.T., Daily, J.W., and Hammitt, F.G., 1970. *Cavitation*. McGraw-Hill, New York.

- [3] Arcoumanis, C., Badami, M., Flora, H. and Gavaises, M., 2000. "Cavitation in Real-size Multi-hole Diesel Injector Nozzles". SAE paper 2000-01-1249.
- [4] Batchelor, G.K., 1980. *An Introduction to Fluid Dynamics*. Cambridge Univ. Press, Cambridge.
- [5] Bergwerk, W., 1959. "Flow Pattern in Diesel Nozzle Spray Holes". Proc. Inst. Mech. Engineers, **173** (25), pp. 655 – 660.
- [6] Nurick, W.H., 1976. "Orifice Cavitation and Its effect on Spray Mixing". ASME, J. Fluids Engineering, **98**, pp. 681 – 687.
- [7] Soteriou, C., Andrews, R., and Smith, M., 1995. "Direct Injection Diesel Sprays and the Effect of Cavitation and Hydraulic Flip on Atomisation". SAE paper 950080.
- [8] Stinebring, D.R., Billet, M.L., Lindau, J.W. and Kunz, R.F., 2001. "Developed Cavitation – Cavity Dynamics". *VKI Lecture Series on Supercavitating Flows*. VKI Press, Brussels.
- [9] Martynov, S.B., Mason, D.J., and Heikal, M.R. 2006. "Numerical Simulation of Cavitation Flows Based on Their Hydrodynamic Similarity". Int. J. of Engine Research, **7** (3), pp. 283 – 296.
- [10] Martynov, S, Mason, D, Heikal, M, Sazhin, S. and Gorokhovski, M. (2006) "Modelling of Cavitation Flow in a Nozzle and Its Effect on Spray Development." *Proc. of the 13th International Heat Transfer Conference*, Australia, Sydney.
- [11] Berthelot, M., 1850. "Sur quelques phenomenes de dilation forcee de liquides". Ann. De Chimie et de Physique, **30**, pp. 232 – 237.

- [12] Joseph, D.D., 1995. “Cavitation in a Flowing Liquid”. *Phys. Review, E.*, **51** (3), pp. 1649 – 1650.
- [13] Joseph, D.D., 1998. “Cavitation and the State of Stress in a Flowing Liquid”, *J. Fluid Mech.*, **366**, pp. 367 – 378.
- [14] Roosen, P, Unruh, O., and Behmann M., 1996. “Untersuchung und Modelierung des transienten Verhaltens von Kavitationserscheinungen bei ein- und mehrkomponentigen Kraftstoffen in schnell durchstromten Dusen”. Report of the Institute for Technical Thermodynamics. RWTH Aachen (Univ. of Tech.), Germany.
- [15] Yuan, W., Sauer, J., and Schnerr, G.H., 2001. “Modelling and Computation of Unsteady Cavitation Flows in Injection Nozzles”. *Mécanique and Industries*, **2** (5), pp. 383 – 394.
- [16] Winklhofer, E., Kull, E., Kelz, E., Morozov, A., 2001. “Comprehensive Hydraulic and Flow Field Documentation in Model Throttle Experiments Under Cavitation Conditions”. *Proceedings of the ILASS-Europe Conference*, Zurich, pp. 574 – 579.
- [17] Yakhot, V., Orszag, S. A., Thangham, S., Gatski., T.B. and Speziale, C.G., 1992. “Development of Turbulence Models for Shear Flows by a Double-Expansion Technique”. *Physics of Fluids, A*, **4** (7), pp. 1510 – 1520.
- [18] Rayleigh, Lord, 1917. “On the Pressure Developed in a Liquid During the Collapse of a Spherical Cavity”. *Phil. Mag.*, **34**, pp. 94 – 98.
- [19] Rosten, H.I. and Spalding, D.B., 1986. *Phoenics – Beginner’s Guide and User Manual*. CHAM TR-100.
- [20] Versteeg, H.K. and Malalasekera, W., 1995. *An introduction to computational fluid dynamics: the finite volume method*. Harlow, Longman.

- [21] Malin, M.R. and Waterson, N.P., 1999, "Schemes for Convection Discretisation in Phoenixics". *Phoenixics J.*, **12** (2), pp. 173 – 201.
- [22] Sato, K. and Saito, Y., 2001. "Unstable Cavitation Behaviour in Circular-Cylindrical Orifice Flow". *Proc. of the 4th Int. Symposium on Cavitation CAV2001*, paper 318.
- [23] Singhal, A.K., Athavale, M.M., Li, H., and Jiang Yu., 2002. "Mathematical Basis and Validation of the Full Cavitation Model". *ASME, J. Fluid Eng.* **124** (3), pp. 617 – 624.